Spectroelectrochemical Behavior of Parallel Arrays of Single Vertically-Oriented *Pseudomonas aeruginosa* Cells

Allison R. Cutri[1], Vignesh Sundaresan[2, a)], Joshua D. Shrout[3,4], and Paul W. Bohn[1,2, b)]

[1]Department of Chemistry and Biochemistry, University of Notre Dame, Notre Dame, IN 46556 USA

[2]Department of Chemical and Biomolecular Engineering, University of Notre Dame, Notre Dame, IN 46556 USA

[3]Department of Civil and Environmental Engineering and Earth Sciences, University of Notre Dame, Notre Dame, IN 46556 USA

[4]Department of Biological Sciences, University of Notre Dame, Notre Dame, IN 46556 USA

a) Present address: Department of Chemistry and Biochemistry, University of Mississippi, University, MS 38677

b) Author to whom correspondence should be addressed: pbohn@nd.edu

Summary

Pseudomonas aeruginosa is a Gram-negative opportunistic human pathogen responsible for a number of healthcare-associated infection. It is currently difficult to assess single cell behaviors of *P. aeruginosa* that might contribute to acquisition of antibiotic resistance, intercellular communication, biofilm development, or virulence, because mechanistic behavior is inferred from ensemble collections of cells, thus averaging effects over a population. Here, we develop and characterize a device that can capture and trap arrays of single *P. aeruginosa* cells in individual micropores in order to study their behaviors using spectroelectrochemistry. Focused ion beam milling is used to fabricate an array of micropores in a Au/dielectric/Au/SiO_2-containing multilayer substrate, in which individual micropores are formed with dimensions that facilitate the capture of single *P. aeruginosa* cells in a predominantly vertical orientation. The bottom Au ring is then used as a working electrode to explore the spectroelectrochemical behavior of parallel arrays of individual *P. aeruginosa* cells. Application of step-potential or swept-potential waveforms produces changes in the fluorescence emission that can be imaged and correlated with applied potential. Arrays of *P. aeruginosa* cells typically exhibit three characteristic fluorescence behaviors that are sensitive to nutritional stress and applied potential. The device developed here enables the study of parallel collections of single bacterial cells with well-defined orientational order and should facilitate efforts to elucidate methods of bacterial communication and multidrug resistance at the single cell level.

Introduction

Pseudomonas aeruginosa is a Gram-negative opportunistic human pathogen found in soil and freshwater that is responsible for many healthcare-associated blood, burn, gastrointestinal, and lung infections.[1-4] Infections of this bacterium are difficult to treat, with as many as 13% being caused by multidrug resistant (MDR) bacteria, a situation that resulted in 32,600 cases and 2,500 deaths in 2017 in the U.S. alone.[4] Antibiotic resistance and virulence traits exhibited by *P. aeruginosa* result from multiple mechanisms, including intrinsic production of efflux pumps and catalytic enzymes enabling tolerance to antibiotics, cell signaling and communication through quorum sensing, development of surface-attached biofilms, the production of persister cells, and the secretion of virulence factors such as pyocyanin and other toxins.[5-8]

Because *P. aeruginosa* infections pose a serious threat, understanding mechanistic behavior both at the population level and at the level of single cells, is of great interest. Recently, significant progress has been made toward identifying new drugs and delivery methods as well as pinpointing key resistance mechanisms. For example, Boedicker *et al*. developed a water-in-oil droplet method to simulate high cell density and induce quorum sensing mechanisms involving a single bacterial cell.[9] Haisch and coworkers grew silver nanoparticles directly onto planktonic bacteria and used antibody capture to detect single bacteria with surface-enhanced Raman scattering.[10] Nallathamby *et al*. used plasmonic silver nanoparticles to study the size-dependent transport kinetics of the MexAB-OprM efflux pump, the main transport pump in *P. aeruginosa* with the ability to extrude a variety of antibiotic compounds. They found that the number of nanoparticles taken up into the cell depends on size, over- or under-expression of the pump, and the addition of inhibitors that affect the proton gradient within the pump.[11]

Although significant progress has been made in understanding behavior of *P. aeruginosa* and other clinically-relevant pathogens, there is still much we do not understand. Current methods of characterization constitute a key bottleneck in addressing this challenge. Most methods rely on studying bulk cultures, which necessarily average important information over large numbers of individual cells. Complex environments composed of cells, secreted metabolites, and extracellular polymeric substances (EPS) exhibit different spatial configurations, different stages of individual cell cycles, and respond to external changes differently.[12-14] Advances in optical and electrochemical detection modalities, such as scanning electrochemical microscopy, super-resolution imaging and microscopy, and micro- and nanodevice fabrication, have made it possible to measure heterogeneities over collections of single-entities, *i.e.* molecules, particles, and cells,[15-19] as demonstrated by the work of Bard and Fan,[20,21] Zhang and White,[22] Pan and coworkers[23], and El-Said *et al*. among others.[24] Additionally, optical and electrochemical experiments can be combined to track single molecule, nanoparticle, or enzyme kinetics, as shown by the use of electrochemical zero-mode waveguides to characterize the spectroelectrochemical dynamics of single redox species.[25]

Here we extend these efforts by developing a new device architecture, the micropore electrode array (MEA), that enables the simultaneous spectroelectrochemical imaging and interrogation of well-defined arrays of single cells. The MEA is capable of trapping a large number (>100) of single *P. aeruginosa* cells in a defined (here, vertical) orientation, and probing their spectroelectrochemical behavior, as shown in **Figure 1**. After capture, depicted schematically in **Figure 1(a)**, the trapped cells are irradiated at a wavelength capable of exciting fluorescence; specifically in these experiments the predominant fluorescence arises from flavins within the bacterial membrane. We observe three fluorescence behaviors from the individual cells in these

arrays that are masked in bulk measurements: (1) potential-modulated fluorescence, in which the fluorescence responds to the applied potential, producing either strong or weak emission modulated by potential, (2) transient, high intensity fluorescence events, hereafter referred to as transient fluorescence, which are observed more often at the positive end of the applied potential range, and (3) potential-independent fluorescence behavior, in which the applied potential has no discernable effect on the emission intensity. Interestingly, these cell behaviors are strongly dependent on metabolic state, with cells that have exhausted their reserve of electrons exhibiting bright fluorescence at oxidizing potentials and much reduced intensities at reducing potentials. However, cells in metabolically active states, *e.g.*, freshly collected cells with all metabolic pathways functioning, exhibit fluorescence in which the potential-dependence of the observed fluorescence is reversed, with more intense fluorescence observed at reducing potentials. These behaviors are not unique to *P. aeruginosa*, as they are also observed in *E. coli*.

The development of this device has made it possible to characterize the fluorescence response from collections of planktonic bacterial cells - one cell at a time - thus enabling the observation of behaviors that were previously obscured. The device enables the study of the relation of spectroelectrochemical behavior to various physical and biological perturbations, such as mutations, environmental changes, and differences in growth conditions at a single cell level. This presents new opportunities for understanding the fundamental biology of microbes and, ultimately, shedding light on the relationship between single cell behavior, that is not homogeneous within a population, and the behavior apparent when the entire population is interrogated simultaneously. It should also illuminate the behavior of bacteria incorporated into other organized structures, such as biological fuel cells and biosensors.

Results and Discussion

MEA device characterization

In addition to SEM imaging, both electrochemical and spectroelectrochemical experiments using known concentrations of ferri/ferrocyanide and FMN and FAD were performed to characterize the performance of the MEA device. Electrochemical characterization of the device was carried out using cyclic voltammetry (CV) as shown in **Figure S1**, using increasing concentrations of either $Fe(CN)_6^{3-}$, **Figure S1(a)**, or $Fe(CN)_6^{4-}$, **Figure S1(b)**, in 2 M KNO_3 supporting electrolyte. The bottom Au ring electrode was used as the working electrode, while external Ag/AgCl and Pt wires served as quasi-reference and counter electrodes, respectively. The potential was swept between -0.4 V $\leq E_{appl} \leq$ 0.6 V. In all four experiments, current increases with increasing concentration of analyte, and the voltammograms exhibit a sigmoidal shape consistent with the steady-state behavior expected from recessed ultramicrolectrodes, as demonstrated by White and coworkers.[26]

Next, the MEAs were characterized by observing the spectroelectrochemical behavior of 100 μM flavin species, FMN and FAD, freely diffusing in 0.2 M KNO_3, specifically the fluorescence modulation as a function of potential, as shown in **Figure 2**. An optical image of the MEA for each sample is provided, along with a typical intensity time-trace and associated histogram of a typical single pore. The same potential-time modulation waveform was used for all three samples, 0.2 V $\geq E_{appl} \geq$ -0.8 V at a scan rate of 100 mV s^{-1}. As expected, cyclic sweep fluorescence data for FAD and FMN show high fluorescence intensities at oxidizing potentials and much weaker fluorescence as the potential is scanned to reducing values.[27] Interestingly, the polarity of the potential-modulated fluorescence is just the opposite for captured PAO1c *P. aeruginosa* cells; at oxidizing potentials (0.2 V *vs.* Ag/AgCl), fluorescence intensity is lower

compared to the intensity at reducing values (-0.8 V *vs.* Ag/AgCl), although the depth of modulation is much weaker than it is for free diffusing FMN/FAD.

The weaker fluorescence intensity modulation of single PAO1c *P. aeruginosa* cells compared to freely diffusing flavins can be ascribed to a combination of factors. First, the occupancy of flavin molecules within a single MEA micropore is *ca.* $\langle n_{pore} \rangle \sim 2.4 \times 10^5$, which is much larger than the estimated number of flavins in the bacterial membrane. In addition, diffusion times to reach the working electrode from within the nanopore are ≤ 1 ms, which is fast on the electrochemical timescale. Furthermore, it is probable that, in the absence of a redox mediator, only a fraction of the flavoenzymes in the bacterial membrane are sufficiently close to participate in electron transfer. Both of these considerations argue for stronger modulation of freely diffusing FMN and FAD than for bacterial membrane-bound flavins. Within the bacterial membrane, glucose is converted to pyruvate via the Entner-Doudoroff pathway and in subsequent steps, electrons from pyruvate are transferred to NADH, NADPH, and $FADH_2$ and ultimately on to molecular O_2 as the terminal electron acceptor. The effects of electron transfer down the redox gradient on fluorescence intensity of the flavoenzymes has yet to be fully characterized, but it is certainly reasonable to assert that it will have an effect on bacterial potential-modulated fluorescence that does not exist for freely diffusing FMN and FAD. Finally, we note that, in principle, some pores could contain >1 cell, however, the dimensions of the pore and the working electrode and the optical configuration dictate that the observed fluorescence arises from the single cell at the bottom of the pore.

Potential-dependent fluorescence behaviors in P. aeruginosa

The optimum conditions to load bacteria were initially determined by examining fluorescence images of MEAs as a function of loading time. Differences in intensity levels between scattering from an empty (unloaded) micropore and fluorescence from bacterial-loaded micropores were sufficient to monitor loading. Standard hypothesis testing was used to determine if the signal obtained from a specific micropore varied significantly from the background. Once conditions for optimum bacterial capture and trapping were identified, spectroelectrochemical experiments were implemented. An example of a cyclic potential sweep bacterial fluorescence experiment is shown in **Figure 3**, in which the applied potential was swept in the range +0.2 V > E_{appl} > -0.8 V at 100 mV s^{-1}. This potential range was chosen because flavins undergo redox chemistry in this range, as shown in **Figure S2**. Furthermore, hydrogen bubble formation was ignored, as previous work by Sundaresan *et al*. showed that potentials E_{appl} < -1.5 V *vs.* Ag/AgCl were required to initiate significant bubble formation in nanopores.[28] A representative frame of the recorded movie is shown in **Figure 3(a)**, where each high-intensity spot arises from a pore containing a bacterium near the focal plane. **Figure 3(b)** shows the potential-time trace, while **Figure 3(c)** displays an intensity-time trace integrated over all 121 micropores of the MEA device for this particular applied potential program. The integrated bacterial fluorescence shows a clear potential-dependence, but the overall response hides significant heterogeneity among individual bacteria-containing micropores.

Individual bacterial cells captured in the micropores exhibit one of three distinct patterns of fluorescence response as a function of applied potential: (1) potential-independent fluorescence, **Figures 3(d)** and **3(e)**; (2) potential-modulated fluorescence, **Figures 3(f)** and **3(g)**, or (3) high-intensity fluorescence transients that deviate from a low-level baseline but only last for a few frames, **Figures 3(h)** and **3(i)**. Intensity histograms were used to classify cells in each of the 121

micropores in the array into one of three behavioral pattern groups corresponding to these archetypes, as described below. Potential-independent fluorescence is characterized by a single Gaussian distribution, **Figure 3(e)**, potential-modulated fluorescence can be fit to two overlapping Gaussian distributions, **Figure 3(g)**, and fluorescence profiles containing high-intensity transients are characterized by the appearance of a high-intensity tail, **Figure 3(i)**. The same three fluorescence behavior patterns are observed when the polarity of the cyclic potential sweep is reversed, *e.g.*, starting at E_0 = -0.4 V and sweeping in the range -0.4 V < E_{appl} < +0.6 V. These results are striking, because they reveal that the distinct potential dependence of the array-integrated fluorescence shown in **Figure 3(c)** results from the superposition of three distinct single cell behaviors. These behaviors, normally masked when experiments are performed with bulk planktonic cultures or biofilms, are revealed here, especially the behavior of fluorescence transients, which in a multicell sample might simply be interpreted as excess noise. Finally, we note that there can be significant differences in average fluorescence intensity levels among individual cells in different micropores. We attribute these differences to a combination of cell position - both distance from the working electrode and distance from the focal plane - biological cell-to-cell variation, and optical aberrations, especially spherical aberration.[29,30]

Statistical analysis of fluorescence behavior

Classification of fluorescence behaviors was established by applying specific statistical tests to the fluorescence data in the presence of applied potential steps. For potential-modulated fluorescence, the moving average for each time series was determined and a Student's t-test applied to determine if intensity peak values at 0, 10, 20, 30, 40, 50, and 60 s, *i.e.*, the times at which the potential switched, were different from each other at the 99% confidence level. If this

condition was met, then the behavior was characterized as potential-modulated fluorescence. For data exhibiting putative transient fluorescence events, each data point within a time series was compared to its two nearest neighbors. If a specific point in a time trace was larger than the two neighbors, then the point was identified as a candidate peak. Then, in order to differentiate true fluorescent transients from noise, the overall variance of the time series was determined, and a 3σ condition was applied to identify the transient peaks. Additionally, histograms of transient fluorescence data typically also showed a significant high-intensity tail, depending on the number of transients observed in a particular run. If the intensity-time trace from a single bacterial cell in a pore did not satisfy either the potential-dependent or fluorescence transient criteria, the cell was classified as having potential-independent fluorescence. Micropores exhibiting this behavior likely result from: (*a*) dead bacterial cells, (*b*) cells located at axial positions within the pore where either they could not participate in faradaic electron transfer, or (*c*) cells located sufficiently far from the focal plane that excitation and/or emission could not be detected. Furthermore, to assess the generality of these potential-dependent fluorescence behaviors, MEAs were used to capture and characterize the behavior of single *E. coli* cells, in addition to the *P. aeruginosa* cells used for the majority of the spectroelectrochemical experiments. The results from this analysis are shown in **Figure 4** with specific populations tabulated in **Table 1**. Overall, potential-modulated fluorescence is the most frequently observed behavior, followed by potential-independent fluorescence and fluorescence transients, for both bacteria species. For *P. aeruginosa* species, 63.1% of cells demonstrated potential-modulated fluorescence, 28.8% of cells demonstrated potential-independent fluorescence, and 8.1% of cells demonstrated fluorescence transients. For *E. coli*, the values were 43.4%, 40.7%, and 15.9%, respectively. It is important to note that while the values for *E. coli* are closer, the population size is much smaller as fewer *E. coli* cells were characterized.

Possible sources of fluorescence

Although the classification procedure assesses patterns of potential-dependent fluorescence behavior of single *P. aeruginosa* cells, it does not address the source of the fluorescence. A single bacterial cell is a complex molecular assembly, so it is important to consider which constituents could possibly contribute to the observed signal before interpreting the optical data. There are two critical requirements for the observation of potential-modulated fluorescence from a single bacterial cell: the transfer of electrons with an extracellular medium (electrode) and the availability of electrofluorogenic species capable of excitation/emission at the wavelengths used in the experiment. In the absence of redox mediators that can shuttle electrons through the outer membrane, close ($\leq$ 2 nm) contact between the electrode and the outer bacterial membrane is required.[31] Because the outer membrane of Gram-negative bacteria is inherently insulating, a membrane-resident electron transporter is needed to shuttle electrons across the outer membrane.[32] In *P. aeruginosa* the available transporters are cytochromes, phenazines, quinones, dehydrogenases, and both bound, *e.g.*, as redox cofactors in flavoenzymes, and unbound flavins.[33-35] While all of these can emit fluorescence under the right conditions, most are excited at near-UV wavelengths and minimally at the excitation wavelength, λ = 458 nm, used in these experiments.[6,36-39] Furthermore, a detection bandpass filter blocks emission outside of the 500-575 nm range, where emission of other potential contributors typically occurs. Thus, the species responsible for the observed emission must be excited at 458 nm and emit in the range 500-575 nm.

As an example, the fluorescence signal from 10 μM FMN, **Figures S2(a)** and **S2(b)**, or FAD solutions, **Figures S2(c)** and **S2(d)**, loaded into MEAs elicit readily discernable fluorescence

when excited at 458 nm, while 10 μM pyocyanin, a canonical blue pigment of *P. aeruginosa*, gives only a background response both in the fluorescence image, **Figures S2(e)** and the intensity-time data, **S2(f)**. In addition, a pyocyanin-deficient strain of *P. aeruginosa* exhibits bacterial fluorescence similar to the wild type, **Figure S3**. If pyocyanin or another phenazine were the dominant source of fluorescence observed, fluorescence would not be observed in the *Δphz* mutant. The flavin containing electron carriers FMN and FAD, as well as other flavin-containing biomolecules, such as flavoenzymes, meet all of the above criteria. In addition, there is a possibility that enzymes containing iron-sulfide clusters or ubiquinone might also contribute to the observed fluorescence, as these compounds have similar excitation and emission spectra.[40] In addition, the emission might arise from some uncharacterized chromophore, but this is unlikely for a well-studied species such as *P. aeruginosa*.

Comparison of P. aeruginosa *and* E. coli

In order to address whether the observed potential-dependent fluorescence is characteristic of pseudomonads, or occurs in other bacterial systems, *E. coli* was also investigated using the same potential programs. *E. coli* is also a Gram-negative, rod-shaped bacterium with similar dimensions to *P. aeruginosa* and has been extensively studied, making it an ideal species for comparison, since it is amenable to capture and trapping in the same MEA device architecture used for *P. aeruginosa*. The results of potential-step single bacterial cell fluorescence imaging experiments from the two species are compared in **Figure S4**. All three canonical fluorescence behaviors are observed for single cells of both species, though only potential-modulated fluorescence and fluorescence transient are shown in the figure. In addition, when the signal is integrated over the entire MEA area, both species exhibit potential-modulated integrated fluorescence, similar to that shown in

Figure 3(c). Both species also exhibit the same fluorescence-potential polarity; when the potential is reducing, E_{appl} = -0.4 V, the signal intensity is high, but then decreases once the potential is stepped to an oxidizing value, E_{appl} = +0.6 V, **Figures S4(c)** and **S4(g)**. Single *E. coli* cells also exhibit the fluorescence transient behavior, **Figure S4(h)**, seen in *P. aeruginosa*, **Figure S4(d)**, signifying that the observed behaviors are not unique to pseudomonads.

Metabolic state dependence

Alkyl quinolones (AQs), including Pseudomonas quinolone signal (PQS), correlate with both population density and stress. Previously, our laboratories used hyperspectral Raman chemical imaging to examine the temporal and spatial profiles of AQs secreted by *P. aeruginosa* under metabolic stress, effected by carbon limitation, and found that it resulted in accelerated PQS production.[41] This led us to ask whether metabolic stress might also be reflected in potential-dependent bacterial fluorescence. Cells freshly collected from a phase of exponential growth in the presence of abundant carbon and other nutrients are metabolically-active. However, in the absence of an exogenous carbon source, the electron storage reserves accumulated must be consumed to ensure bacterial metabolism. Eventually, the reserve of reducing equivalents is nearly exhausted, and the cells are metabolically-inactive, as the electron transport chain is not able to support aerobic growth.

To explore this question, we carried out experiments on metabolically-active and inactive cells in the presence of a redox mediator, 5 mM methyl viologen (MV^{2+}) in 0.2 M KNO_3, to ensure effective electronic communication between the electrode and the bacterial cell as well as relaxing the requirement for strict physical proximity. Potential step experiments, E_{appl} = +0.2 V to -0.8 V

vs. Ag/AgCl, were performed, and two significant differences were noted. While both metabolically-active and metabolically-inactive cells demonstrate all three fluorescence behaviors (although only potential-modulated fluorescence is shown in **Figure 5**, the change in fluorescence intensity between oxidizing and reducing potentials is much stronger for metabolically-inactive cells, *cf.* **Figures 5(c)** and **5(f)**, and the separation of the peaks in the histogram is much larger, *cf.* **Figures 5(d)** and **5(g)**. The same dichotomy in the behavior of metabolically-active and inactive cells is observed when the potential is stepped between E_{appl} = -0.4 V to +0.6 V (data not shown). In addition to the differences between metabolically-active and inactive cells, these experiments utilizing MV^{2+} redox mediator display a striking difference in the polarity of the potential dependence. Independent of metabolic state, emission intensities are higher in the presence of positive applied potentials than negative potentials, as shown in **Figures 5(c)** and **5(f)**, although the effect is much clearer in the metabolically-inactive cells. This behavior is in contrast to the potential-dependent polarity in the absence of mediator, as shown in **Figures 3(f)** and **3(g)**.

The differences between the behavior of metabolically-active and inactive cells likely reflect differences in the ability of the bacteria to utilize electron transport chains based on metabolic condition. Furthermore, the presence of a redox mediator adds another mechanism by which the bacterial cells can communicate with the solid working electrode. Thus, the differences in the behaviors under these two sets of conditions may be determined by an interplay between these two sets of factors.

We have successfully fabricated and characterized an optically-accessible micropore electrode array device capable capturing and trapping a parallel array of orientationally ordered single bacterial cells. The device is ideally suited to spectroelectrochemical characterization of single bacterial cells, as demonstrated here with *P. aeruginosa* and *E. coli*. The effect of potential

on bacterial fluorescence response is characterized by three patterns of behavior: (*a*) potential-modulated fluorescence, where are the florescence intensity level follows the electrochemical potential, (*b*) sporadic fluorescence transients, in which the intensity increases transiently to a peak height than 3σ from the local baseline; and (*c*) potential-independent florescence. These single-cell fluorescence behaviors are completely masked in ensemble measurements.

Based on the excitation and emission conditions and the requirement for close physical proximity to support efficient electron transfer, much of the fluorescence signal likely arises from flavin-containing species, such as flavoenzymes and unbound flavins. The appearance of the same three behaviors in *E. coli* as well as *P. aeruginosa* is consistent with the presence of the same molecular constituents across bacterial species. The observation of potential-modulated fluorescence is consistent with flavin-based redox processes, and a putative origin of the intense fluorescence transients is put forward. Finally, significant differences in the potential-dependent fluorescence behavior of single *P. aeruginosa* cells are observed between metabolically-active and inactive cells and in the presence and absence of redox mediator. The mechanisms behind these behaviors are currently under investigation in our laboratory.

The ability to trap and monitor single cells in parallel opens the door to many opportunities, such as studies of the effect of growth conditions and environmental stress on spectroelectrochemical behavior. Building on these single cell potential-dependent fluorescence experiments and incorporating additional imaging approaches, like confocal Raman microscopy and single-cell electrochemical surface-enhanced Raman spectroscopy (EC-SERS), it may be possible to elucidate details of cell signaling and multidrug resistance mechanisms that are of great interest.

Experimental Procedures

Lead Contact

Further information and requests for resources can be provided by the lead contact, Paul W. Bohn (pbohn@nd.edu).

Materials availability

All materials mentioned in this study can be made upon reasonable request to the lead contact.

Data and code availability

Experimental data can be found within the article or supplementary information. Data processing and statistical analysis were performed using Matlab. Code is openly available at https://github.com/acutri5396/Micropore-electrode-array-processing, DOI:10.5281/zenodo.7702597.

Supporting Information:

Supporting information is available on the Publications website and contains:

- Experimental procedures; MEA device characterization; FMN and FAD control experiments; comparison between FMN, FAD, and pyocyanin fluorescence; multipotential step experiments using metabolically-active and -inactive PAO1c cells with a positive

applied potential range; comparison of fluorescence transients with negative vs. positive potential ranges.

Acknowledgments:

This work was supported by the National Institute of Allergies and Infectious Diseases through grant R01AI113219.6 and by the National Science Foundation through grant CHE-1904196. The authors gratefully acknowledge the Notre Dame Nanofabrication Facility and Notre Dame Integrated Imaging Facility for providing fabrication and characterization support.

Author Contributions:

ARC contributed to Methodology, Validation, Formal Analysis, Investigation, Writing (Original Draft, Review, and Editing), and Visualization. VS contributed to Methodology, Validation, Formal Analysis, Writing (Original Draft, Review, and Editing), and Visualization. JDS contributed to Conceptualization, Resources, Writing (Review & Editing), Supervision, Project Administration, and Funding Acquisition. PWB contributed to Conceptualization, Writing (Review & Editing), Supervision, Project Administration, and Funding Acquisition.

Declarations of interests:

There are no conflicts of interest to declare.

References:

1. Talebi Bezmin Abadi, A., Rizvanov, A.A., Haertlé, T., and Blatt, N.L. (2019). World Health Organization Report: Current Crisis of Antibiotic Resistance. BioNanoScience *9*, 778-788. 10.1007/s12668-019-00658-4.
2. Pang, Z., Raudonis, R., Glick, B.R., Lin, T.-J., and Cheng, Z. (2019). Antibiotic resistance in Pseudomonas aeruginosa: mechanisms and alternative therapeutic strategies. Biotechnol. Adv. *37*, 177-192. 10.1016/j.biotechadv.2018.11.013.
3. Pachori, P., Gothalwal, R., and Gandhi, P. (2019). Emergence of antibiotic resistance Pseudomonas aeruginosa in intensive care unit; a critical review. Genes & Diseases *6*, 109-119. https://doi.org/10.1016/j.gendis.2019.04.001.
4. CDC (2019). Antibitotic Resistance Threats in the United States, 2019. 2019.
5. Smith, R.S., and Iglewski, B.H. (2003). P. aeruginosa quorum-sensing systems and virulence. Curr. Opin. Microbiol. *6*, 56-60. https://doi.org/10.1016/S1369-5274(03)00008-0.
6. Das, T., Kutty, S.K., Tavallaie, R., Ibugo, A.I., Panchompoo, J., Sehar, S., Aldous, L., Yeung, A.W.S., Thomas, S.R., Kumar, N., et al. (2015). Phenazine virulence factor binding to extracellular DNA is important for Pseudomonas aeruginosa biofilm formation. Sci. Rep. *5*, 8398. 10.1038/srep08398.
7. Hall, S., McDermott, C., Anoopkumar-Dukie, S., McFarland, A.J., Forbes, A., Perkins, A.V., Davey, A.K., Chess-Williams, R., Kiefel, M.J., Arora, D., and Grant, G.D. (2016). Cellular Effects of Pyocyanin, a Secreted Virulence Factor of Pseudomonas aeruginosa. Toxins (Basel) *8*. 10.3390/toxins8080236.
8. Strateva, T., and Yordanov, D. (2009). Pseudomonas aeruginosa-a phenomenon of bacterial resistance. J. Med. Microbiol. *58*, 1133-1148. 10.1099/jmm.0.009142-0.
9. Boedicker, J.Q., Vincent, M.E., and Ismagilov, R.F. (2009). Microfluidic Confinement of Single Cells of Bacteria in Small Volumes Initiates High-Density Behavior of Quorum Sensing and Growth and Reveals Its Variability. Angew. Chem. Int. Ed. *48*, 5908-5911. 10.1002/anie.200901550.
10. Zhou, H., Yang, D., Mircescu, N.E., Ivleva, N.P., Schwarzmeier, K., Wieser, A., Schubert, S., Niessner, R., and Haisch, C. (2015). Surface-enhanced Raman scattering detection of bacteria on microarrays at single cell levels using silver nanoparticles. Microchim Acta *182*, 2259-2266. 10.1007/s00604-015-1570-0.
11. Nallathamby, P.D., Lee, K.J., Desai, T., and Xu, X.H.N. (2010). Study of the multidrug membrane transporter of single living pseudomonas aeruginosa cells using size-dependent plasmonic nanoparticle optical probes. Biochemistry *49*, 5942-5953. 10.1021/bi100268k.
12. Schuler, B., and Hofmann, H. (2013). Single-molecule spectroscopy of protein folding dynamics—expanding scope and timescales. Curr. Opin. Struct. Biol. *23*, 36-47. 10.1016/j.sbi.2012.10.008.
13. Weaver, W.M., Tseng, P., Kunze, A., Masaeli, M., Chung, A.J., Dudani, J.S., Kittur, H., Kulkarni, R.P., and Di Carlo, D. (2014). Advances in high-throughput single-cell microtechnologies. Curr. Opin. Biotechnol. *25*, 114-123. 10.1016/j.copbio.2013.09.005.

14. Baker, L.A. (2018). Perspective and Prospectus on Single-Entity Electrochemistry. Journal of the American Chemical Society *140*, 15549-15559. 10.1021/jacs.8b09747.
15. Yu, Y., Sun, T., and Mirkin, M.V. (2015). Scanning Electrochemical Microscopy of Single Spherical Nanoparticles: Theory and Particle Size Evaluation. Anal. Chem *87*, 18. 10.1021/acs.analchem.5b01690.
16. Yabiku, Y., Kubo, S., Nakagawa, M., Vacha, M., and Habuchi, S. (2013). Super-resolution fluorescence imaging of nanoimprinted polymer patterns by selective fluorophore adsorption combined with redox switching. AIP Advances *3*, 102128. 10.1063/1.4827155.
17. Moerner, W.E., Shechtman, Y., and Wang, Q. (2015). Single-molecule spectroscopy and imaging over the decades. Faraday Discuss. *184*, 9-36. 10.1039/c5fd00149h.
18. Sandison, M.E., and Cooper, J.M. (2006). Nanofabrication of electrode arrays by electron-beam and nanoimprint lithographies. Lab on a Chip *6*, 1020-1025. 10.1039/b516598a.
19. Sharma, D., Lee, J., Seo, J., and Shin, H. (2017). Development of a sensitive electrochemical enzymatic reaction-based cholesterol biosensor using Nano-sized carbon interdigitated electrodes decorated with gold nanoparticles. Sensors (Switzerland) *17*, 1-8. 10.3390/s17092128.
20. Fan, F.-R.F., and Bard, A.J. (1995). Electrochemical Detection of Single Molecules. Science *267*, 871-874. 10.1126/science.265.5168.46.
21. Fan, F.-R.F., Kwak, J., and Bard, A.J. (1996). Single Molecule Electrochemistry. Journal of the American Chemical Society *118*, 9669-9675.
22. Zhang, B., Zhang, Y., and White, H.S. (2004). The nanopore electrode. Anal. Chem. *76*, 6229-6238. 10.1021/ac049288r.
23. Hill, C.M., Bennett, R., Zhou, C., Street, S., Zheng, J., and Pan, S. (2015). Single Ag Nanoparticle Spectroelectrochemistry via Dark-Field Scattering and Fluorescence Microscopies. J. Phys. Chem. C. *119*, 6760-6768. 10.1021/jp511637a.
24. El-Said, W.A., Kim, T.-H., Chung, Y.-H., and Choi, J.-W. (2015). Fabrication of new single cell chip to monitor intracellular and extracellular redox state based on spectroelectrochemical method. Biomaterials *40*, 80-87. 10.1016/j.biomaterials.2014.11.023.
25. Han, D., Crouch, G.M., Fu, K., Zaino, L.P., and Bohn, P.W. (2017). Single-molecule spectroelectrochemical cross-correlation during redox cycling in recessed dual ring electrode zero-mode waveguides. Chem. Sci. *8*, 5345-5355. 10.1039/c7sc02250f.
26. Zhang, B., Zhang, Y., and White, H.S. (2004). The nanopore electrode. Anal. Chem.
27. Zaino, L.P.I., Grismer, D.A., Han, D., Crouch, G.M., and Bohn, P.W. (2015). Single Molecule Spectroelectrochemistry of Freely Diffusing Flavin Mononucleotide in Zero-Dimensional Nanophotonic Structures. Faraday Disc. *184*, 101-115.
28. Sundaresan, V., and Bohn, P.W. (2020). Acid–base chemistry at the single ion limit. Chemical Science *11*, 10951-10958. 10.1039/d0sc03756g.

29. Gelber, M.K., Kole, M.R., Kim, N., Aluru, N.R., and Bhargava, R. (2017). Quantitative Chemical Imaging of Nonplanar Microfluidics. Anal. Chem. *89*, 1716-1723. 10.1021/acs.analchem.6b03943.
30. Michielsen, S. (2001). Aberrations in confocal spectroscopy of polymeric materials: Erroneous thicknesses and intensities, and loss of resolution. J. Appl. Polym. Sci. *81*, 1662-1669. 10.1002/app.1597.
31. Aiyer, K.S. (2020). How does electron transfer occur in microbial fuel cells? World J. Microbiol. Biotechnol. *36*, 19. 10.1007/s11274-020-2801-z.
32. Baron, D., LaBelle, E., Coursolle, D., Gralnick, J.A., and Bond, D.R. (2009). Electrochemical Measurement of Electron Transfer Kinetics by Shewanella oneidensis MR-1. J. Biol. Chem. *284*, 28865-28873. 10.1074/jbc.M109.043455.
33. Kracke, F., Vassilev, I., and Kromer, J.O. (2015). Microbial electron transport and energy conservation - the foundation for optimizing bioelectrochemical systems. Front. Microbiol. *6*. 10.3389/fmicb.2015.00575.
34. Hernandez Maria, E., Kappler, A., and Newman Dianne, K. (2004). Phenazines and Other Redox-Active Antibiotics Promote Microbial Mineral Reduction. Applied and Environmental Microbiology *70*, 921-928. 10.1128/AEM.70.2.921-928.2004.
35. Rabaey, K., Boon, N., Höfte, M., and Verstraete, W. (2005). Microbial Phenazine Production Enhances Electron Transfer in Biofuel Cells. Environ. Sci. Technol. *39*, 3401-3408. 10.1021/es048563o.
36. Briard, B., Bomme, P., Lechner, B.E., Mislin, G.L.A., Lair, V., Prévost, M.-C., Latgé, J.-P., Haas, H., and Beauvais, A. (2015). Pseudomonas aeruginosa manipulates redox and iron homeostasis of its microbiota partner Aspergillus fumigatus via phenazines. Sci. Rep. *5*, 8220. 10.1038/srep08220.
37. Bräm, O., Consani, C., Cannizzo, A., and Chergui, M. (2011). Femtosecond UV Studies of the Electronic Relaxation Processes in Cytochrome *c*. J. Phys. Chem. B *115*, 13723-13730. 10.1021/jp207615u.
38. Perinbam, K., Chacko Jenu, V., Kannan, A., Digman Michelle, A., and Siryaporn, A. (2020). A Shift in Central Metabolism Accompanies Virulence Activation in Pseudomonas aeruginosa. mBio *11*, e02730-02718. 10.1128/mBio.02730-18.
39. Hodgkinson, J.T., Gross, J., Baker, Y.R., Spring, D.R., and Welch, M. (2016). A new Pseudomonas quinolone signal (PQS) binding partner: MexG. Chem. Sci. *7*, 2553-2562. 10.1039/c5sc04197j.
40. Rungrassamee, W. (2008). Oxidative stress responses in *Escherichia coli* and *Pseudomonas aeruginosa.* Ph.D. Thesis (University of Massachusetts Amherst).
41. Cao, T., Sweedler Jonathan, V., Bohn Paul, W., and Shrout Joshua, D. (2020). Spatiotemporal Distribution of Pseudomonas aeruginosa Alkyl Quinolones under Metabolic and Competitive Stress. mSphere *5*, e00426-00420. 10.1128/mSphere.00426-20.

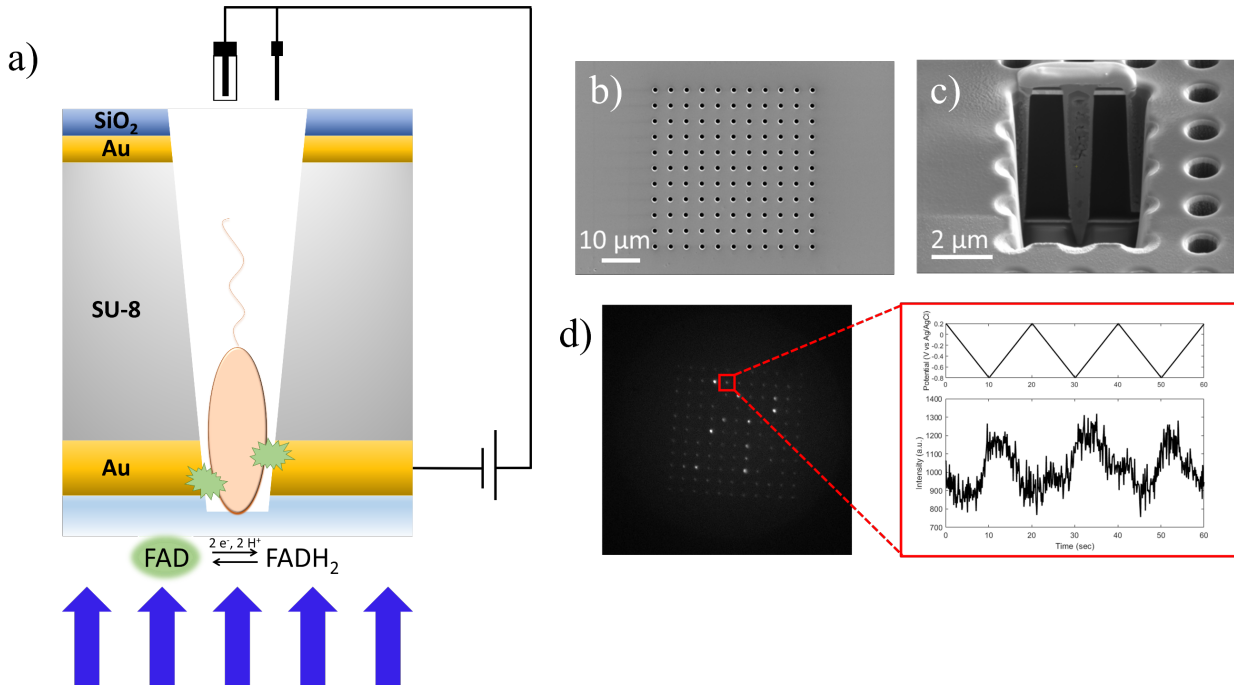

Figure 1. Micropore electrode array (MEA). **(a)** Schematic cross-sectional representation of a single micropore designed to capture a single rod-shaped bacterial cell and monitor its spectroelectrochemical behavior. An electrochemical potential is applied to the bottom Au electrode where the bacterial cell resides, and the device is illuminated from below. Fluorescence is collected in an inverted epi-illumination geometry and directed to an EMCCD camera. External Ag/AgCl and Pt wires serve as quasi-reference and counter electrodes, respectively. **(b)** Plan view and **(c)** cross-sectional (52º tilt) SEM images of the fabricated array. The two Au layers (light) are distinguished from the SU-8 spacer (dark). **(d)** Single frame image from one experimental movie. High intensity locations represent fluorescence from single bacterial cells captured in single micropores. Potential dependent single cell fluorescence intensity-time traces are obtained for all pores simultaneously, as illustrated at right for the pore outlined in red.

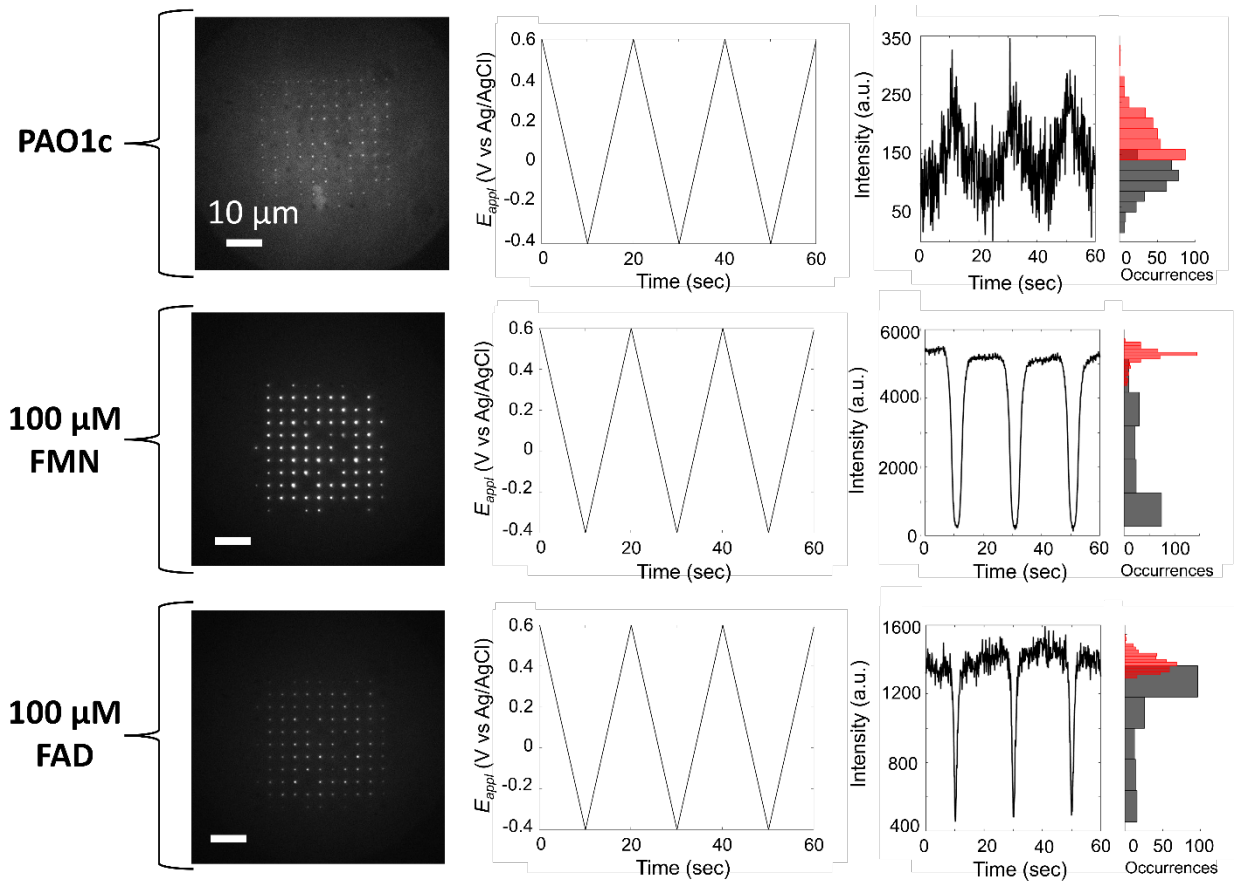

Figure 2. Spectroelectrochemical characterization in an MEA device. PAO1c single cell behavior (top row) is compared to that of freely-diffusing 100 µM FMN (middle row) and 100 µM FAD (bottom row) in 0.2 M KNO_3 supporting electrolyte. First column: fluorescence images of MEAs with the indicated sample. Second column: potential-time modulation waveform. Third column: fluorescence intensity *vs.* time under potential modulation. Fourth column: intensity histograms colored to reflect the high (red) and low (gray) fluorescence intensity states.

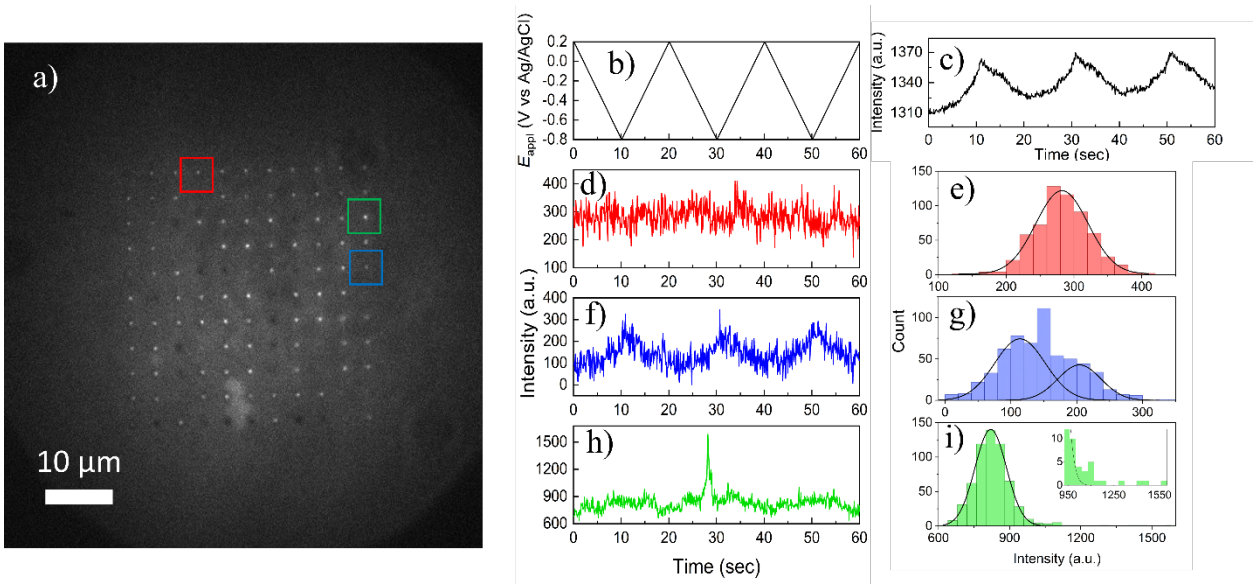

Figure 3. Cyclic potential sweep single bacterial cell fluorescence. **(a)** Representative 100 ms frame taken from a 60 s movie, with a cyclic potential waveform applied to the bottom electrode. High intensity locations correspond to micropores containing fluorescent bacteria. Red, green, and blue boxes correspond to the single micropore intensity-time traces and histograms of the same color. **(b)** Applied potential as a function of time. **(c)** Intensity-time trace integrated over all micropores in the MEA. **(d)** Single bacterium exhibiting potential-independent fluorescence response, and **(e)** corresponding histogram. **(f)** Single bacterial cell exhibiting potential-modulated fluorescence and **(g)** corresponding histogram. **(h)** Single bacterial cell exhibiting transient high-intensity fluorescent transients and **(i)** corresponding histogram. (*Inset*) Expanded view of the high intensity tail of the histogram. Solid lines in panels **(e)**, **(g)**, and **(i)** are fits of the observed histograms to 1 (**(e)** and **(i)**) or 2 **(g)** Gaussian distributions.

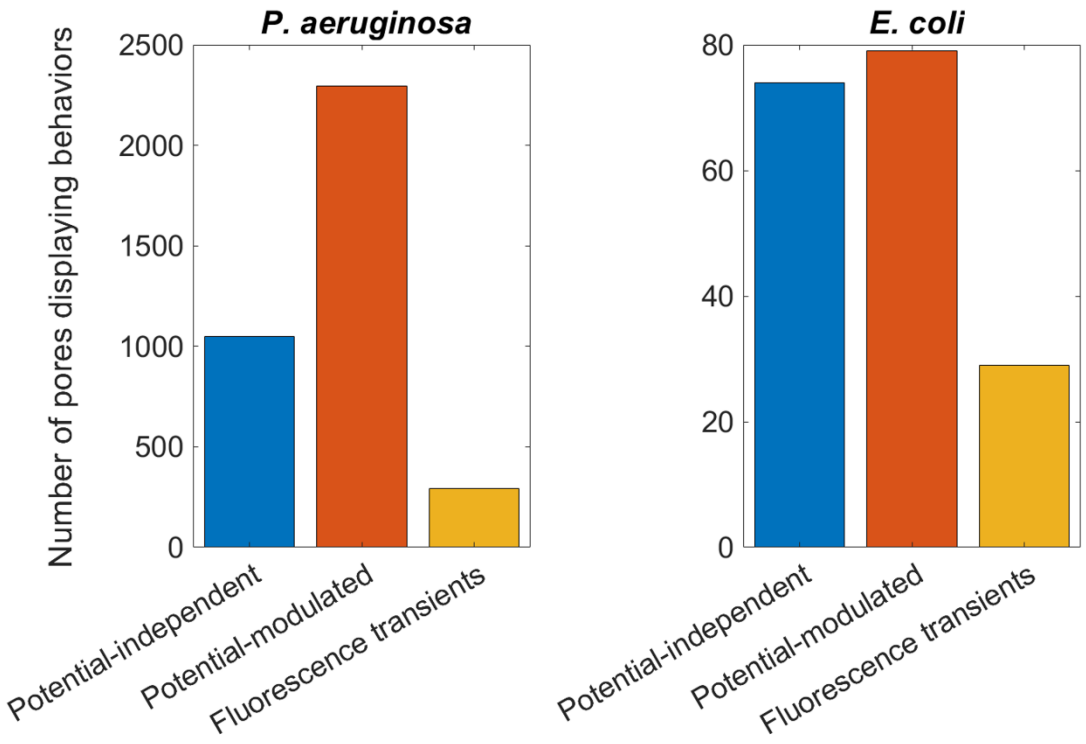

Figure 4. Distribution of fluorescence behaviors for both *P. aeruginosa* (left) and *E. coli* (right). The *P. aeruginosa* histogram contains data for all strains studied (PAO1c, PA14, *Δphz*).

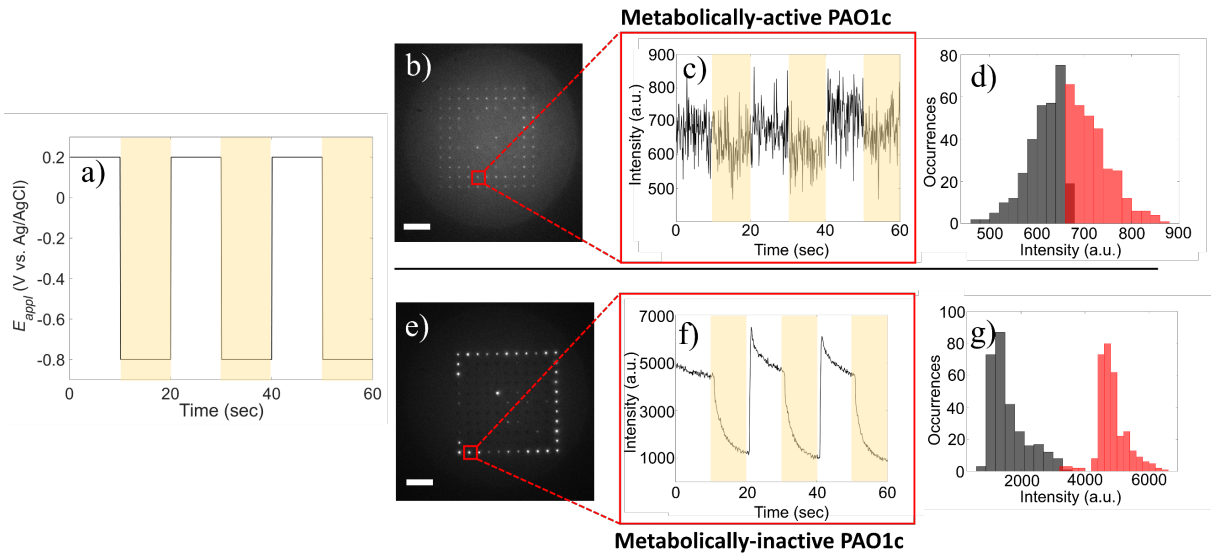

Figure 5. Comparison between metabolically-active and inactive bacteria in the MEA device in the presence of MV^{2+} redox mediator. **(a)** Potential time-trace used in the potential step experiments. **(b)** Single frame image recorded for metabolically-active bacteria. Scale bar is 10 µm. **(c)** Intensity time-trace for the single bacterium highlighted in the red square. White/orange regions represent times of positive/negative applied potential, respectively. **(d)** Histogram of intensities plotted to accentuate the low-intensity (gray) and high-intensity (red) fluorescence levels. **(e)** Single frame image recorded for metabolically-inactive bacteria. Scale bar is 10 µm. **(f)** Intensity time-trace for the single bacterium highlighted in the red square. **(g)** Histogram of intensities plotted to accentuate the low-intensity (gray) and high-intensity (red) fluorescence levels.

Table 1. **Single cell potential-dependent fluorescence behavior by species.**

Fluorescence Behavior	*P. aeruginosa* [a]	*E. coli*
Potential-independent	1,048	74
Potential-modulated	2,295	79
Fluorescence transients	294	29

[a]*P. aeruginosa* data contains data for all strains studied (PAO1c, PA14, *Δphz*).

TOC Figure:

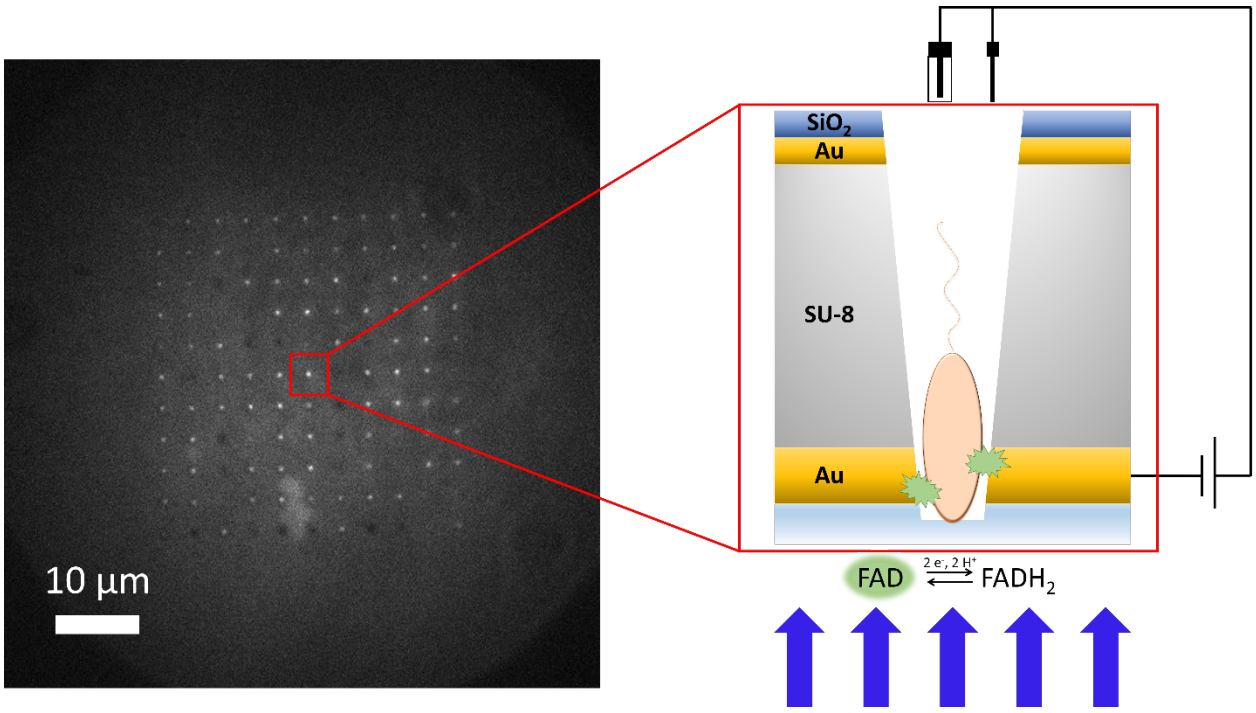

Supplemental Experimental Procedures

Chemicals and materials

Two bacterial species were used in these experiments: *P. aeruginosa* (PAO1c wild type, PA14 wild type, and PA14 *Δphz*) and *E. coli* (K12 wild type). Potassium ferricyanide ($K_3Fe(CN)_6$), potassium ferrocyanide ($K_4Fe(CN)_6$), potassium nitrate (KNO_3), potassium chloride (KCl), methyl viologen (MV), riboflavin 5′-monophosphate sodium salt hydrate (flavin mononucleotide, FMN), flavin adenine dinucleotide (FAD), pyocyanin (PYO), sodium phosphate dibasic heptahydrate, and citric acid were purchased from Sigma-Aldrich. Dulbecco's 1x phosphate buffered saline (1x PBS) was obtained from Lonza. Silver conductive epoxy was purchased from Electron Microscopy Sciences. Devcon clear 5-minute epoxy was purchased from Fischer Scientific, and a two-part hydroxy-terminated polydimethylsiloxane elastomer was obtained from Polymer Sources, Inc. SU-8 2005 and SU-8 developer were obtained from Kayaku Advanced Materials. Armour Etch glass etchant was purchased from Amazon. All solutions were prepared using deionized (DI) water, $\rho \sim 18.2$ MΩ cm, prepared on a Millipore Milli-Q System. All reagents and solutions were used without further purification, with the exception of 1x PBS, which was photobleached for 24 hours prior to use.

Substrate Fabrication and Characterization

The MEA substrate was prepared on Schott Nexterion cleanroom-cleaned glass slides (Glass D, 75.6 x 25.0 x 0.170 mm, Applied Microarrays) as shown schematically in **Figure S5**. Briefly, a 10 nm Ti adhesion layer and 200 nm Au electrode were deposited onto glass using electron-beam evaporation (Oerlikon 450B evaporator) through a shadow mask purchased from

FrontRange Photomask to form the bottom working electrode. Contact lithography was used to form an approximately 5 μm spacer layer of SU-8 2005 photoresist. This size was chosen to accommodate a typical mature single *P. aeruginosa* cell, which is ≤ 3 μm in length. The device was then placed on a hot plate at 180ºC to cross-link the photoresist layer. A second gold layer, comprised of 10 nm Ti and 100 nm Au, was then deposited using electron-beam evaporation through a shadow mask oriented at a 90º angle to the first layer, such that the two electrode layers overlap in a 200 μm x 200 μm square forming the target area for the MEA micropores. This second Au layer was added to serve as the conductive layer for focused ion beam (FIB)-milling, which cannot be conducted directly on the insulating SU-8 2005 layer. A 120 nm layer of SiO_2 was then deposited using plasma-enhanced chemical vapor deposition (PECVD, Unaxis 790 series, PlasmaTherm) to serve as a protective layer and to facilitate wetting and pore filling. An array of micropores was then patterned in the 200 μm × 200 μm Au overlap area by FIB-milling (FEI, Helios Dual-Beam FIB). The 11×11 array of micropores was prepared with dimensions capable of trapping single *P. aeruginosa* or *E. coli* cells, *i.e.*, pores with typical bottom diameter 0.6-0.7 μm can only admit a single cell in proximity to the bottom electrode. If a second cell becomes immobilized, it is constrained to reside at the mouth of the pore where it is: (*a*) not in electrochemical contact with the bottom ring working electrode, and (*b*) far out of the focal region where it might be observed spectroscopically. Pores exhibit a center-to-center pore distance of 4 μm over a total array area of 25 μm × 25 μm. SEM images of the device in plan view and in cross-section at 52º tilt are given in **Figures 1(b)** and **1(c)**, respectively, obtained at an accelerating voltage of 5kV and an electron beam current of either 0.2 or 0.4 nA. To complete the substrate, a copper wire was attached to the bottom Au layer to provide electrical contact to the working electrode using silver conductive epoxy, and a PDMS well to hold the analyte solution was affixed

to the top surface of the substrate using clear 5-minute epoxy. Electrochemical characterization of the device was performed using 10 μM FMN in 0.2 M KNO_3 and 10 μM FAD in 0.2 M KNO_3 at pH 4, 6, and 8, as shown in **Figure S6**.

Bacteria Preparation and Culture

All bacteria were prepared by initially streaking onto a Luria-Bertani (LB) agar plate after which they were allowed to incubate for 24 h at 37ºC. A single colony was collected and resuspended in 6 mL FAB medium with 30 mM glucose carbon source and allowed to grow at 37ºC with shaking at 240 rpm for 18 h. After an appropriate growth time, 1 mL of this medium containing planktonic cells was collected, and optical density measurement at 600 nm, OD_{600} ~ 1.0, was obtained for an approximate cell count of 10^9 mL^{-1}.[41] The cells were then washed three times in photobleached 1x PBS and centrifuged at 3000 rpm for 5 min to remove any potential fluorescent impurities. The cells were re-suspended, and 100 μL of the washed cell suspension was placed in contact with the assembled MEA device in order to load bacteria into the micropores. After 3 h, the solution was removed, and the MEA device was washed with fresh PBS to remove any adherent cells on the exterior surface.

Spectroelectrochemical Measurements

The device, thus loaded with single *P. aeruginosa* cells was mounted on an Olympus IX-71 inverted epi-illumination microscope fitted with a 100x oil-immersion objective (NA = 1.45, Olympus). A fresh 100 μL aliquot of photobleached 1x PBS (containing no bacteria) was added to the PDMS well to serve as supporting electrolyte. A quasi-Ag/AgCl (q-Ag/AgCl) reference

electrode and Pt counter electrode were then placed into the well, and the device was connected to a potentiostat (CH750E, CH Instruments). The MEA device was illuminated at 458-nm, and fluorescence emission was collected back through the microscope objective, passed through a dichroic filter, and imaged onto a Peltier-cooled EMCCD (Andor iXon EMCCD) with an integration time of 0.1 s. A schematic diagram of the experimental apparatus is shown in **Figure S7**.

Supplemental Figures

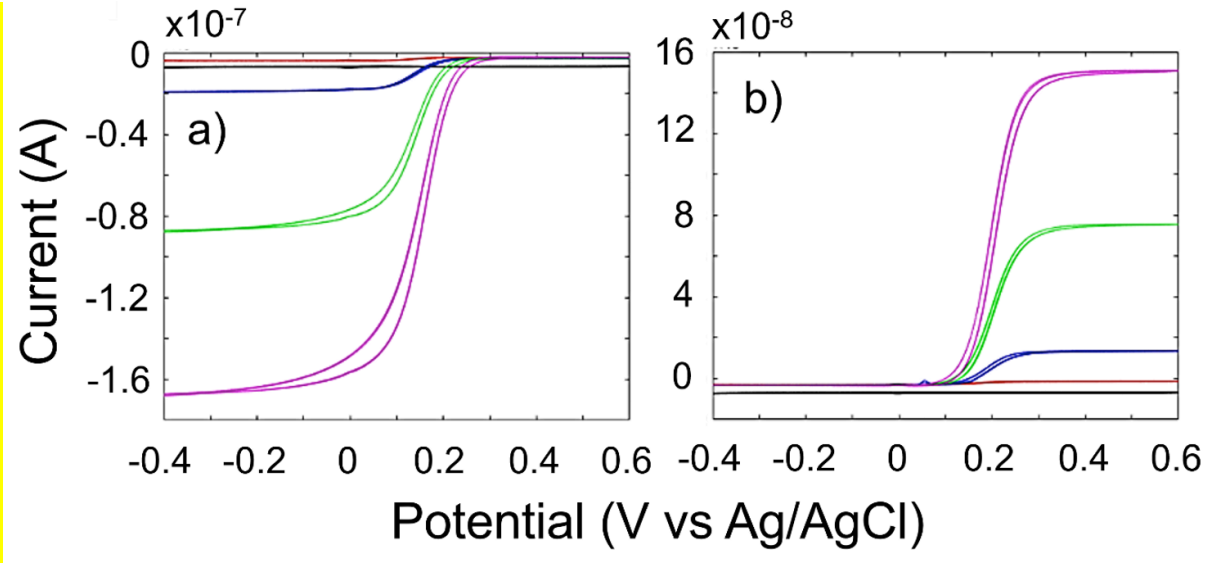

Figure S1. Electrochemical characterization of MEA device using 10 mM $Fe(CN)_6^{3-}$ (a) and $Fe(CN)_6^{4-}$ (b) at 100 mV/s using cyclic voltammetry (CV). The black, red, blue, green, and purple curves represent 0 mM (control), 1 mM, 10 mM, 50 mM, and 100 mM of the redox species, respectively. All CVs were obtained in 2 M KNO_3.

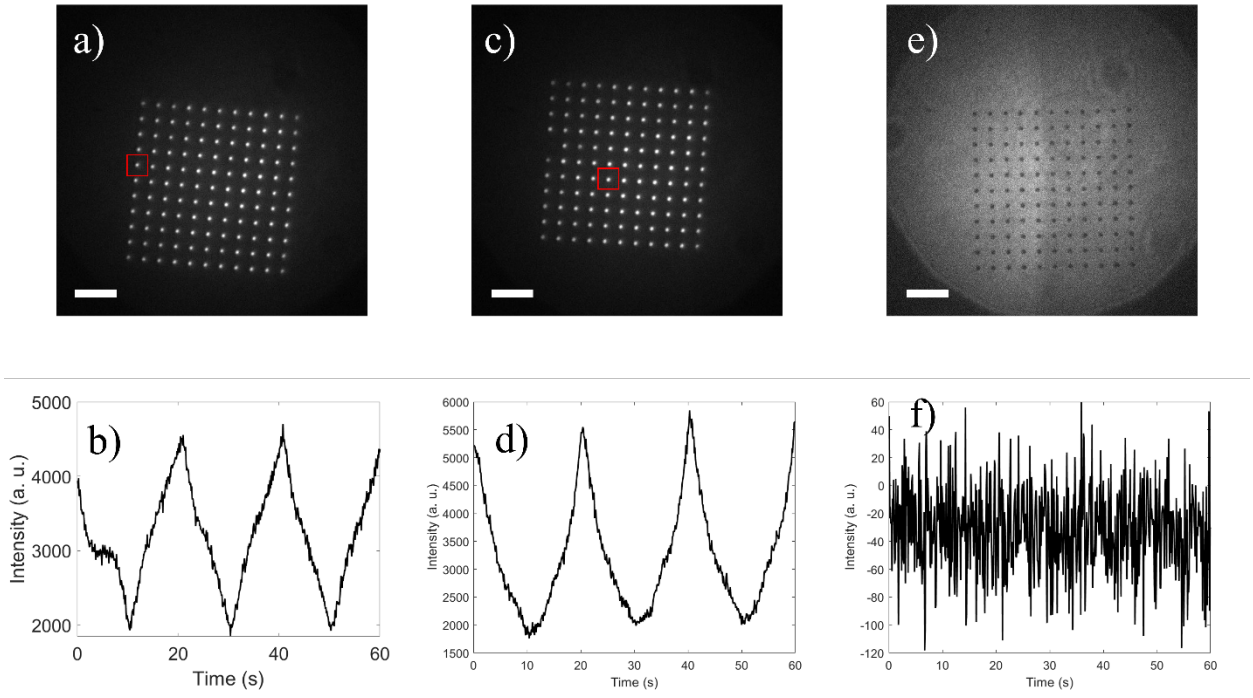

Figure S2. Single frame images and associated single micropore (red square) intensity time-traces for: (a) and (b) 10 μM FMN, (c) and (d) 10 μM FAD, and (e) and (f) 10 μM pyocyanin with the applied potential cycled between +0.2 V > E_{appl} > -0.8 V at a scan rate of 100 mV/s. Fluorescence was excited at λ = 458 nm. Scale bars are 10 μm.

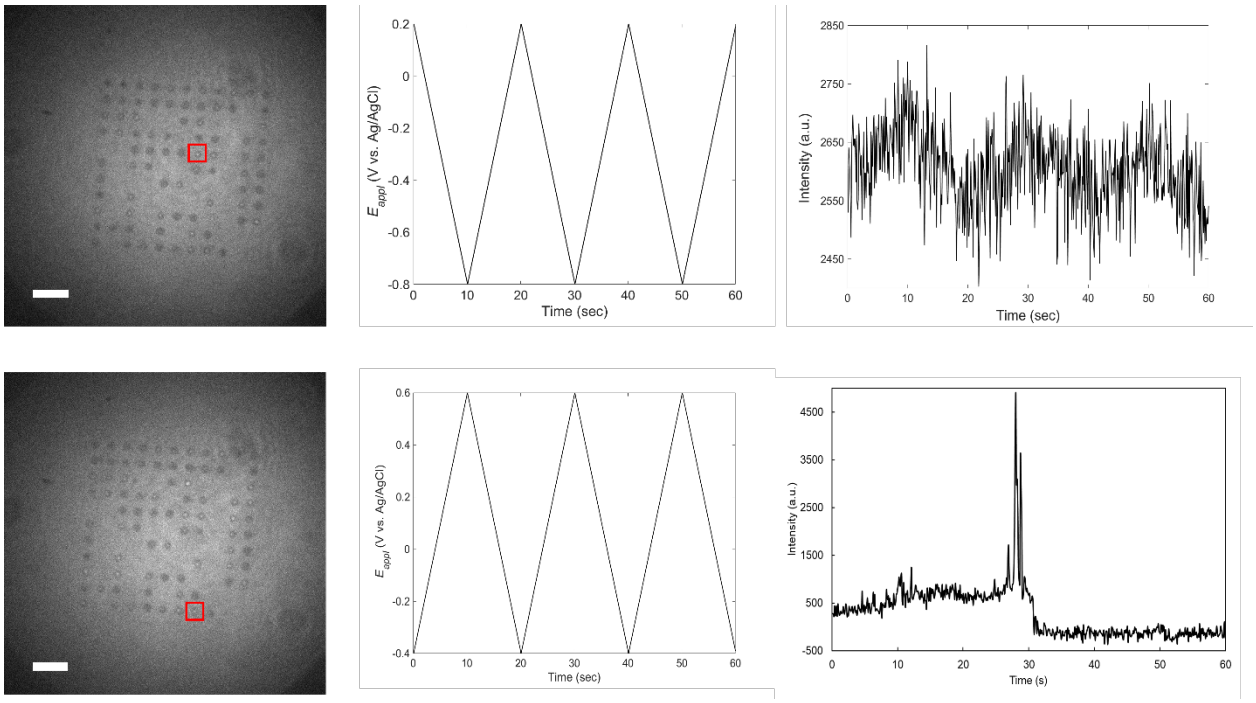

Figure S3. Single frame image (*left*), potential program (*center*) and associated single micropore (red square) intensity time-trace (*right*) for the *Δphz* mutant of *P. aeruginosa*. The top row demonstrates potential-modulated fluorescence with the applied potential cycled between +0.2 V and -0.8 V at a scan rate of 100 mV/s, while the bottom row demonstrates fluorescence transients with the applied potential cycled between -0.4 V and +0.6 V at a scan rate of 100 mV/s. Scale bar is 10 μm.

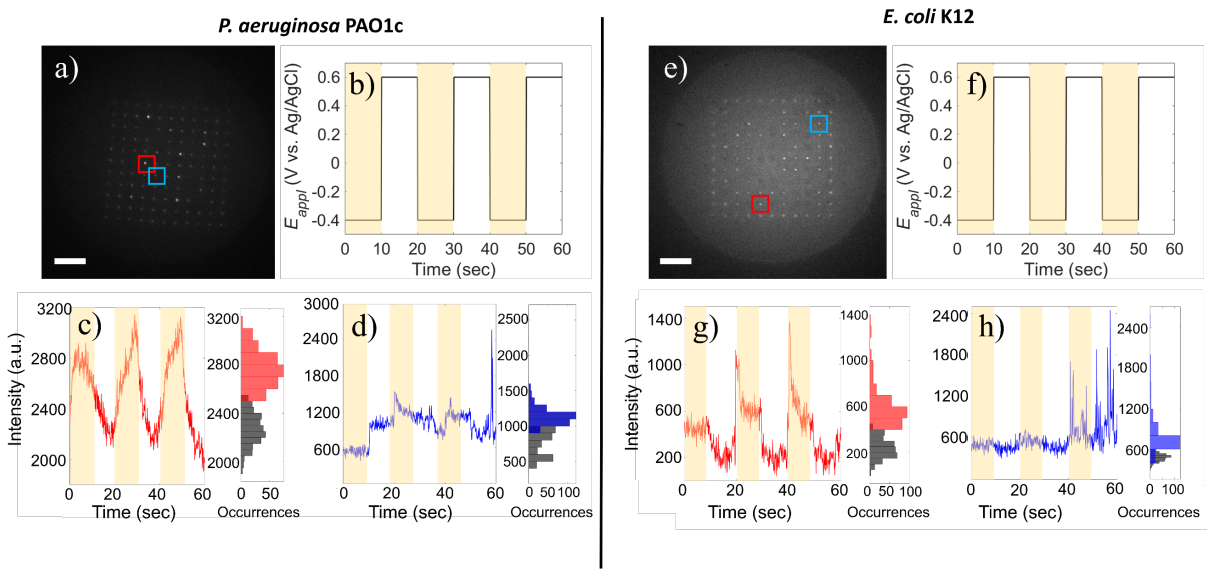

Figure S4. Comparison of *P. aeruginosa* PAO1c (**a-d**) and *E. coli* K12 (**e-h**) spectroelectrochemical behaviors. **(a)** and **(e)** Single movie frame images. **(b)** and **(f)** Potential time-traces for multi-potential step experiment. **(c)** and **(g)** Intensity time-traces for single bacterium outlined in red exhibiting potential-modulated fluorescence behavior. The corresponding histogram is plotted to accentuate the low-intensity (gray) and high-intensity (red) fluorescence levels. **(d)** and **(h)** Intensity time-traces for single bacterium outlined in blue exhibiting fluorescence transient behavior. The corresponding histogram is plotted to accentuate the low-intensity (gray) and high-intensity (blue) fluorescence levels with a high intensity tail. Scale bars are 10 μm.

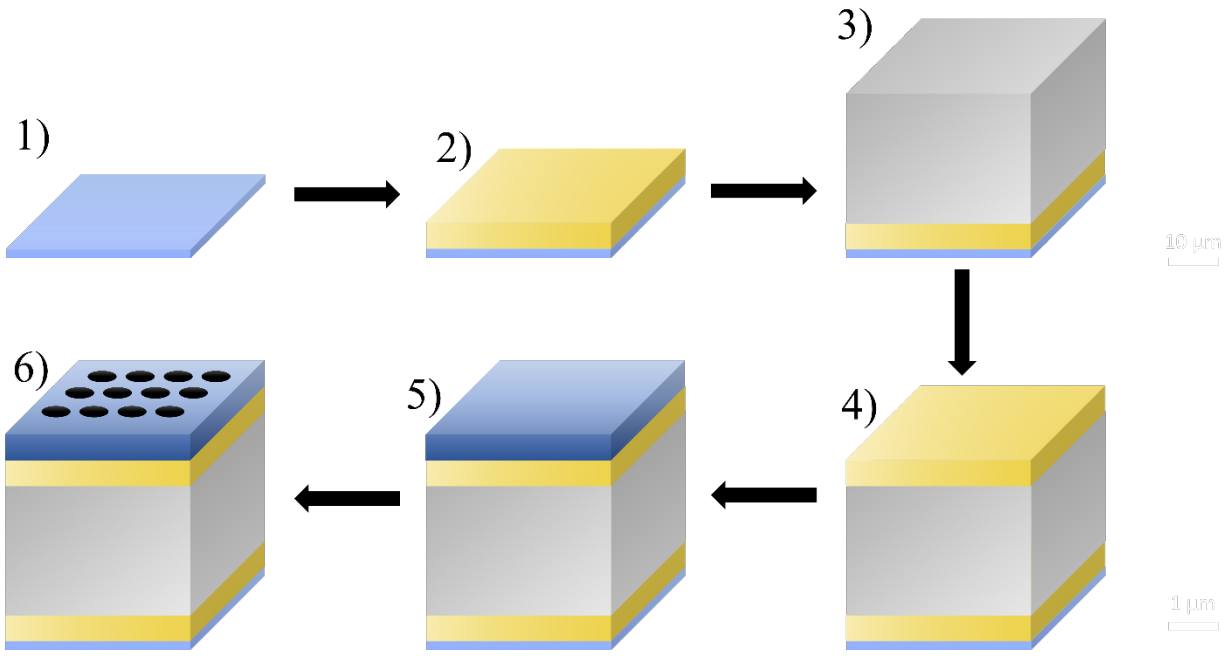

Figure S5: Schematic diagram illustrating fabrication of an MEA device. Clockwise from top left: (1) Start with clean glass slide; (2) deposit 10 nm Ti and 200 nm Au through a shadow mask by electron-beam evaporation; (3) spin-coat, develop, and cross-link a 5 µm spacer layer of SU-8 2005 by contact lithography; (4) deposit 10 nm Ti and 100 nm Au by electron-beam evaporation; (5) deposit 120 nm layer of SiO_2 by plasma-enhanced chemical vapor deposition; (6) direct-write the micropore array using focused-ion beam milling.

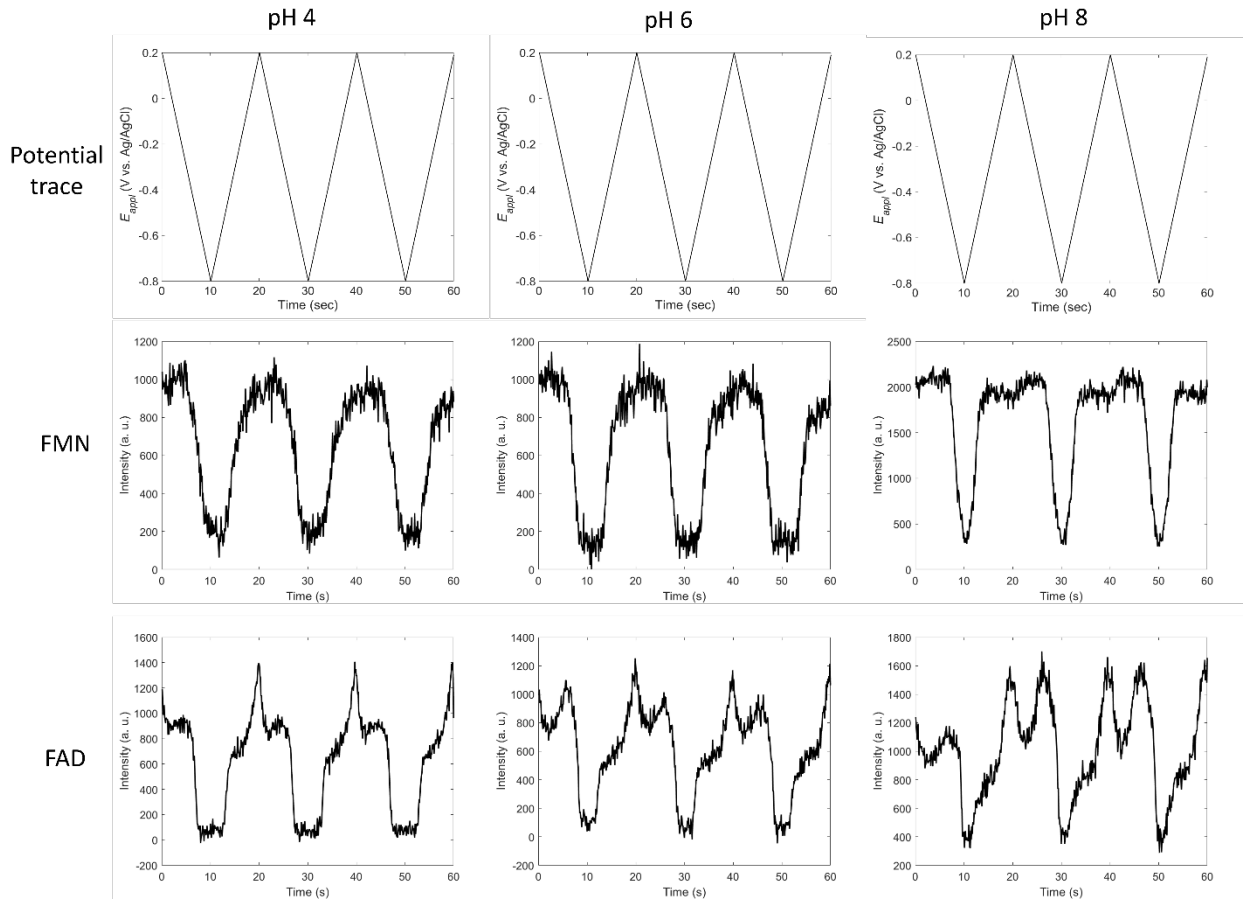

Figure S6. Potential-dependent fluorescence of freely diffusing 10 μM FMN (top row) and 10 μM FAD (bottom row) in 1x PBS. Applied potential was cycled between +0.2 V > E_{appl} > -0.8 V at a scan rate of 100 mV/s (top row) at three different pH values. FAD and FMN are fluorescent at oxidizing potentials and non-fluorescent at reducing potentials independent of pH.

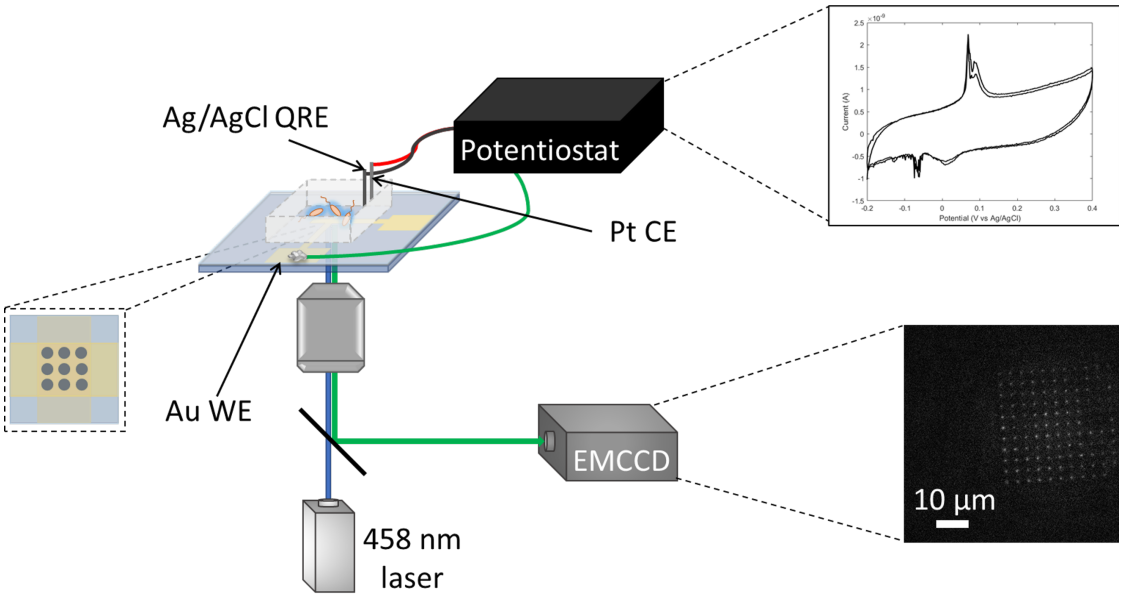

Figure S7. Schematic diagram illustrating the wide-field spectroelectrochemical fluorescence apparatus. The MEA device loaded with cells is placed on an inverted microscope and illuminated from underneath with a 458-nm laser. The subsequent fluorescence is collected through the objective and imaged on an EMCCD camera.